PERGAMON

Journal of Structural Geology 25 (2003) 1107–1120

JOURNAL OF STRUCTURAL GEOLOGY

www.elsevier.com/locate/jsg

Modes of detachment at the inclusion–matrix interface

Susanta Kumar Samanta*, Gautam Bhattacharyya

Department of Geological Sciences, Jadavpur University, Kolkata 700032, India

Received 11 October 2001; received in revised form 17 September 2002; accepted 18 September 2002

Abstract

With the help of a 2D theoretical model, this paper analyses the modes of matrix detachment around a circular–elliptical rigid inclusion under pure and simple shear bulk deformations. Three modes of matrix detachment are possible: *Mode 1*—the matrix is displaced normal to the inclusion boundary, forming fissures at the interface; *Mode 2*—the matrix slips along the inclusion boundary without any separation; *Mode 3*—the detachment occurs by a combination of Modes 1 and 2. In order to determine the onset of detachment at any point on the coherent inclusion–matrix interface, the tensile and shear stresses were derived at that point, and compared with imposed critical values. Numerical simulations based on the theoretical model reveal that the three modes occur systematically along the inclusion–matrix interface, the geometrical dispositions of which depend on the aspect ratio (R) and orientation (ϕ) of the inclusion. In the case of circular inclusions, Mode 1 and Mode 2 domains are separated by a Mode 3 domain and the disposition shows an internal symmetry. On the other hand, it is asymmetrical when the inclusions are elliptical and oriented oblique to the bulk extension direction in pure shear and to the shear direction in simple shear. In simple shear, Mode 2 detachment with synthetic slip occurs dominantly when ϕ is less than 45° and greater than 135°. The results obtained from numerical models are complemented with observations in physical experiments. The paper also determines theoretically the critical stresses for detachment to occur as a function of R for different ϕ values, revealing that for a given mechanical strength of the inclusion–matrix interface, a particular mode of detachment can take place only when the aspect ratio crosses a threshold value.

Keywords: Detachment; Inclusion–matrix interface; Tensile stress; Shear stress

1. Introduction

In a rock system containing rigid inclusions, the inclusion–matrix interface may be coherent or incoherent during deformation (Ramsay and Huber, 1983, p. 265). In the case of an incoherent interface the matrix may be separated from the inclusion or slip along the interface. Models of the heterogeneous flow field around rigid inclusions and development of inclusion-related structures such as drag folds, porphyroclast tails, porphyroblast inclusion trails, strain shadows etc. are based on coherent (non-slip) or incoherent (slip) matrix–inclusion interfaces (Gay, 1968; Masuda and Ando, 1988; Bjornerud, 1989; Passchier, 1994; Bjornerud and Zhang, 1995; Masuda and Mizuno, 1996; Ramsay and Lisle, 2000; Mandal et al., 2001a). Theoretical and experimental studies suggest that the assumption of the mechanical condition at the inclusion–matrix interface could significantly influence the pattern of heterogeneous deformation around the inclusion (Ildefonse and Mancktelow, 1993; Kenkmann and Dresen, 1998; Pennacchioni et al., 2000; Mancktelow et al., 2002). This in turn is likely to modify the development of various inclusion-related structures. For example, the pattern of mantle structures around rigid porphyroclasts changes from σ to δ type with increase in the degree of coherence between the porphyroclast and the matrix (Bjornerud and Zhang, 1995).

Studies mentioned above deal with the effect of inclusion–matrix coherence on the deformation around the inclusions. However, how the coherence at the inclusion–matrix interface is lost leading to detachment is yet to be investigated in detail. This paper analyses development of detachments under the heterogeneous stress field in the neighbourhood of an inclusion. It can be shown that the detachment may occur principally in three modes (Fig. 1). *Mode 1*: the matrix gets detached from the inclusion with displacement normal to the inclusion–matrix interface, forming fissures at the interface (cf. Ramsay and Huber, 1983, p. 265). *Mode 2*: the matrix slips along the

* Corresponding author.
E-mail address: susanta_ju@hotmail.com (S.K. Samanta).

0191-8141/03/$ - see front matter © 2002 Elsevier Science Ltd. All rights reserved.
PII: S0191-8141(02)00157-8

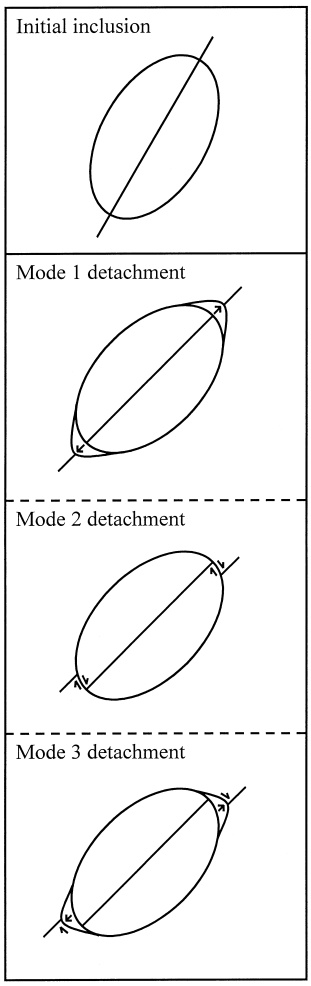

Fig. 1. Modes of matrix detachment around rigid inclusions (details in text).

surface of the inclusion without any creation of gap. *Mode 3*: the matrix detachment occurs by a combination of Modes 1 and 2. These three contrasting modes of detachment are demonstrated in simple physical model experiments. With the help of a 2D theory, the traction that develops at the inclusion–matrix interface in response to the heterogeneous flow around the inclusion are determined in order to analyse the three modes of detachment under simple and pure shear deformations. Numerical simulations based on the theory were performed to reveal the distribution of different modes of detachment around the inclusion as a function of its shape and orientation.

2. Theoretical analysis

The presence of an inclusion leads to a heterogeneous flow field around the inclusion, which in turn exerts traction on the surface of the inclusion. The inclusion–matrix interface becomes locally incoherent where the traction reaches the (adhesive) strength of coherence between the inclusion and matrix. Thus, formulation of the traction acting along the inclusion–matrix interface is the fundamental step for analysing the conditions of inclusion–matrix detachment. In order to do this, we have adopted Jeffery's (1922) theory that describes the flow field around an ellipsoidal inclusion. However, in the present study, for the sake of simplicity, the analysis is made in two dimensions, considering a single, elliptical inclusion floating in an infinitely extended ductile matrix. An outline of the analysis is given below.

Consider an elliptical inclusion with semi-axes a and b, within a viscous matrix undergoing a general deformation by a combination of pure shear and simple shear at rates, $\dot{\epsilon}_b$ and $\dot{\gamma}_b$. A Cartesian reference, oxy, is chosen with the origin at the centre of the inclusion and x-axis parallel to the bulk shear direction (Fig. 2). The principal extension of the pure shear component is assumed to be oriented along the x-axis. The long axis of the inclusion is oriented at angle ϕ with the shear direction. We consider another reference, $ox'y'$, with the x'-axis fixed to the a-axis of the inclusion. Now, with respect to oxy the bulk strain-rate tensor can be represented by the following matrix:

$$\epsilon_{ij} = \begin{bmatrix} \dot{\epsilon}_b & \dot{\gamma}_b/2 \\ \dot{\gamma}_b/2 & -\dot{\epsilon}_b \end{bmatrix} \tag{1}$$

The Eigen values of the matrix give the principal strain rates in the flow as:

$$\dot{\epsilon}_p = \pm \frac{1}{2}\dot{\gamma}_b\sqrt{1+4S_r^2} \tag{2}$$

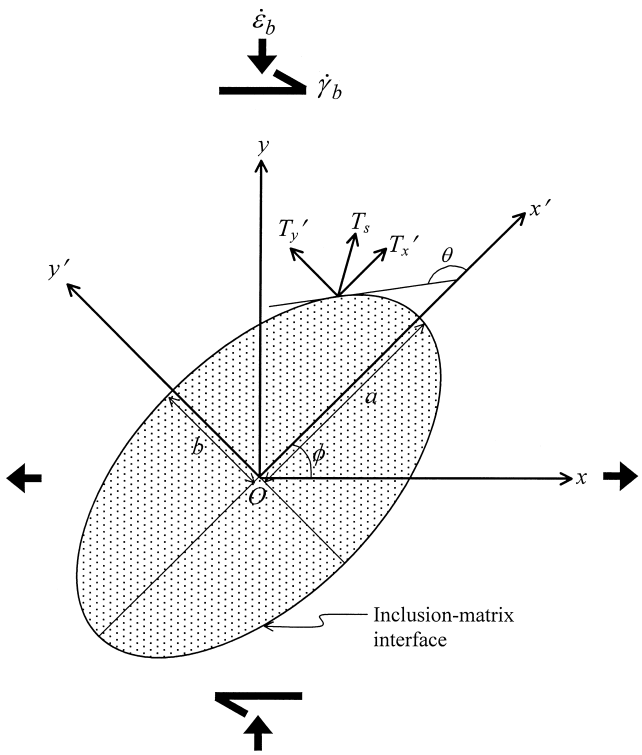

Fig. 2. Consideration of Cartesian co-ordinate frames for theoretical analysis. T_s is the traction vector at a point on the surface of the inclusion and $T_{x'}$ and $T_{y'}$ are its components along the axial directions of the inclusion.

where $S_r = \dot{\epsilon}_b/\dot{\gamma}_b$, the ratio of pure and simple shear rates. In this analysis we require a transformation of the tensor in Eq. (1) with respect to $ox'y'$. From the rule of second-rank tensor transformation, it follows that:

$$S_{pq} = l_{pi}l_{qj}\epsilon_{ij}, \tag{3}$$

where S_{ij} is the strain-rate tensor with respect to $ox'y'$ and

$$l_{ij} = \begin{bmatrix} \cos\phi & \sin\phi \\ -\sin\phi & \cos\phi \end{bmatrix} \tag{4}$$

From Eqs. (3) and (4), we have the components of S_{ij} as:

$$s_{11} = \gamma_b\left(S_r\cos2\phi + \frac{1}{2}\sin2\phi\right) \tag{5a}$$

$$s_{22} = -\gamma_b\left(S_r\cos2\phi + \frac{1}{2}\sin2\phi\right) \tag{5b}$$

$$s_{12} = \gamma_b\left(\frac{1}{2}\cos2\phi - S_r\sin2\phi\right) \tag{5c}$$

The viscous flow in the matrix develops traction on the surface of the inclusion. At any point the traction vector T_s can be given by:

$$T_s = \begin{bmatrix} T_{x'} \\ T_{y'} \end{bmatrix} \tag{6}$$

where $T_{x'}$ and $T_{y'}$ are the components of the traction parallel to the axial directions of the inclusion (Fig. 2). Following Jeffery's (1922) theory, their expressions can be written as:

$$T_{x'} = P\left(L\frac{x'}{a^2} + M\frac{y'}{b^2}\right) \tag{7a}$$

$$T_{y'} = P\left(M'\frac{x'}{a^2} + L'\frac{y'}{b^2}\right) \tag{7b}$$

where

$$\frac{1}{P^2} = \frac{x'2}{a^4} + \frac{y'2}{b^4}.$$

The expressions of the constants in Eqs. (7a) and (7b) follow (after Mandal et al., 2001b):

$$L = -p_o + 4\eta\left\{\frac{2}{ab} - (\alpha_o - \beta_o)\right\}A,\ M = \frac{8\eta}{ab}H$$

$$L' = -p_o - 4\eta\left\{\frac{2}{ab} + (\alpha_o - \beta_o)\right\}A,\ M' = \frac{8\eta}{ab}H' \tag{8}$$

where p_o and ω are the confining pressure and the co-efficient of viscosity of the matrix, respectively. In Eq. (8) the expressions of the parameters are:

$$A = \frac{S_{11}}{2[(\alpha_o + \beta_o) - (a^2 + b^2)\gamma_o]}$$

$$H = \frac{\alpha_o S_{12} - \gamma_o b^2(S_w - \omega)}{2(\alpha_o a^2 + \beta_o b^2)\gamma_o}$$

$$H' = \frac{\beta_o S_{12} + \gamma_o a^2(S_w - \omega)}{2(\alpha_o a^2 + \beta_o b^2)\gamma_o} \tag{9}$$

where ω is the instantaneous rate of rotation of the inclusion, the expression of which is (Eq. (39) of Jeffery, 1922):

$$\omega = \frac{a^2(S_w + S_{12}) + b^2(S_w - S_{12})}{a^2 + b^2} \tag{10}$$

$S_w = \dot{\gamma}_b/2$, the rotation component of the bulk flow:

$$\alpha_o = \frac{2}{a(a+b)},\ \beta_o = \frac{2}{b(a+b)} \text{ and } \gamma_o = \frac{2}{ab(a+b)^2} \tag{11}$$

The derivations of Eqs. (8)–(11) can be found in Mandal et al. (2001b). After some algebraic manipulations of these equations, the expressions of the constants in Eqs. (7a) and (7b) are obtained:

$$L = -p_o + 2\eta\left(\frac{a+b}{b}\right)S_{11}$$

$$L' = -p_o - 2\eta\left(\frac{a+b}{a}\right)S_{11}$$

$$M = M' = 2\eta\frac{(a+b)^2}{a^2+b^2}S_{12} \tag{12}$$

We shall now consider the traction components normalised to the bulk flow stress, and rewrite Eqs. (7a) and (7b) as:

$$T^*_{x'} = P\left(L^*\frac{x'}{a^2} + M^*\frac{y'}{b^2}\right)$$

$$T^*_{y'} = P\left(M'*\frac{x'}{a^2} + L'*\frac{y'}{b^2}\right) \tag{13}$$

where

$$L^* = \frac{L}{2\eta\dot{\epsilon}_p},\ L'* = \frac{L'}{2\eta\dot{\epsilon}_p} \text{ and } M^* = M'* = \frac{M}{2\eta\dot{\epsilon}_p} \tag{14}$$

Replacing the expressions of L, L' and M' and $\dot{\epsilon}_p$ in Eq. (14), and after some simplifications, we have:

$$L^* = -p^*_o + (1+R)\frac{\sin2\phi + 2S_r\cos2\phi}{\sqrt{1+4S_r^2}}$$

$$L^* = -p^*_o - \left(1 + \frac{1}{R}\right)\frac{\sin2\phi + 2S_r\cos2\phi}{\sqrt{1+4S_r^2}}$$

$$M^* = \frac{(R+1)^2}{R^2+1}\frac{\cos2\phi - 2S_r\sin2\phi}{\sqrt{1+4S_r^2}} \tag{15}$$

where R is the aspect ratio of the inclusion. Eqs. (13) and (15) indicate that the aspect ratio R and the orientation ϕ of the inclusion are the principal parameters governing the traction of the matrix on the surface of the inclusion. Now, the normal (σ_n) and shear (σ_t) stress components at any point on the surface of the inclusion can be obtained from

the traction vector by using the following equation:

$$\begin{bmatrix} \sigma_t^* \\ \sigma_n^* \end{bmatrix} = \begin{bmatrix} \cos\theta & \sin\theta \\ -\sin\theta & \cos\theta \end{bmatrix} \begin{bmatrix} T_{x'}^* \\ T_{y'}^* \end{bmatrix} \quad (16)$$

where θ is the slope of the tangent to the inclusion boundary, the expression of which follows:

$$\theta = -\tan^{-1}\left(\frac{b^2}{a^2}\frac{x'}{y'}\right) \quad (17)$$

It is evident from Eqs. (13)–(17) that the normal and shear stress components acting on the inclusion–matrix interface will be different at different points, and result in detachment between the inclusion and matrix where their values exceed the strength of cohesion between the matrix and inclusion. In our analysis we express the mechanical strength of the inclusion–matrix interface by tensile strength (T_o) and shear strength (S_o) independently. The dynamic conditions of the three modes of detachment are:

Mode 1: when $\sigma_n^* > T_o^*$, $\sigma_t^* < S_o^*$
Mode 2: when $\sigma_n^* < T_o^*$, $\sigma_t^* > S_o^*$
Mode 3: when $\sigma_n^* > T_o^*$, $\sigma_t^* > S_o^*$

S_o^* and T_o^* are the shear and tensile strengths of the inclusion–matrix interface normalised to the bulk flow stress. By imposing the above conditions we ran numerical experiments by using the traction functions (Eq. (13)) for different shapes and orientations of the inclusion to investigate how detachment occurs at the inclusion–matrix interface. The results are discussed in the following sections.

3. Detachment in numerical models

3.1. Method of simulation

A computer program was developed in Visual Basic to compute the stress components acting on the surface of the inclusion, and to find the points satisfying the dynamic conditions for the three modes of detachment stated in the previous section. In the initial model short radial lines were drawn across the inclusion boundary to reveal the domains of detachment along the inclusion–matrix interface. The magnitude of relative displacement between two adjacent points on either side of the interface was assumed to be directly proportional to the magnitudes of the stress components acting at that point. Experiments were conducted separately under pure shear ($S_r = \infty$), simple shear ($S_r = 0$) and $S_o^* = T_o^* = 1$. In the following sections we present results obtained from pure and simple shear experiments.

3.2. Detachment patterns

A set of numerical simulations was performed under *pure shear* by varying the initial orientation (ϕ) of inclusion for different values of the aspect ratio R.

Circular inclusions ($R = 1$): the inclusions show detachment over a large area, leaving a small intact area of the inclusion–matrix interface facing to the principal shortening direction. The detachment area consists of symmetrically disposed fissures on either side of the inclusion along the bulk extension direction, and slip zones (Mode 2) in the transition between the intact interface and the fissures (Fig. 3a). The central parts of the fissures have developed by Mode 1 detachment, whereas their fringes show Mode 3 detachment (Fig. 3b).

Elliptical inclusions ($R > 1$): sets of experiments were performed by varying the initial orientation (ϕ) of inclusion, keeping the aspect ratio (R) constant. In the case of $R = 2$ and $\phi = 0$ Mode 1 (fissure) detachment occurs symmetrically on its either side (Fig. 4a), as noticed in many naturally deformed rocks. The locales of Mode 1 detachment are flanked by locales of Mode 3 and Mode 2 detachment (Fig.4a). When the inclusion is obliquely oriented with respect to the bulk extension direction,

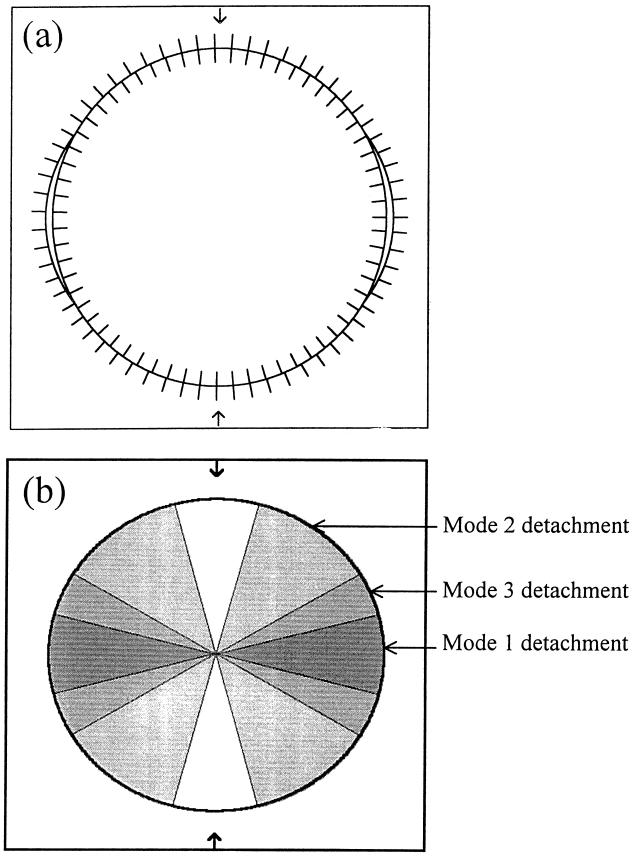

Fig. 3. (a) Pattern of matrix detachment around a circular inclusion in numerical model under pure shear. (b) Calculated plots showing the disposition of the three modes of detachment (shaded) and intact interface (blank).

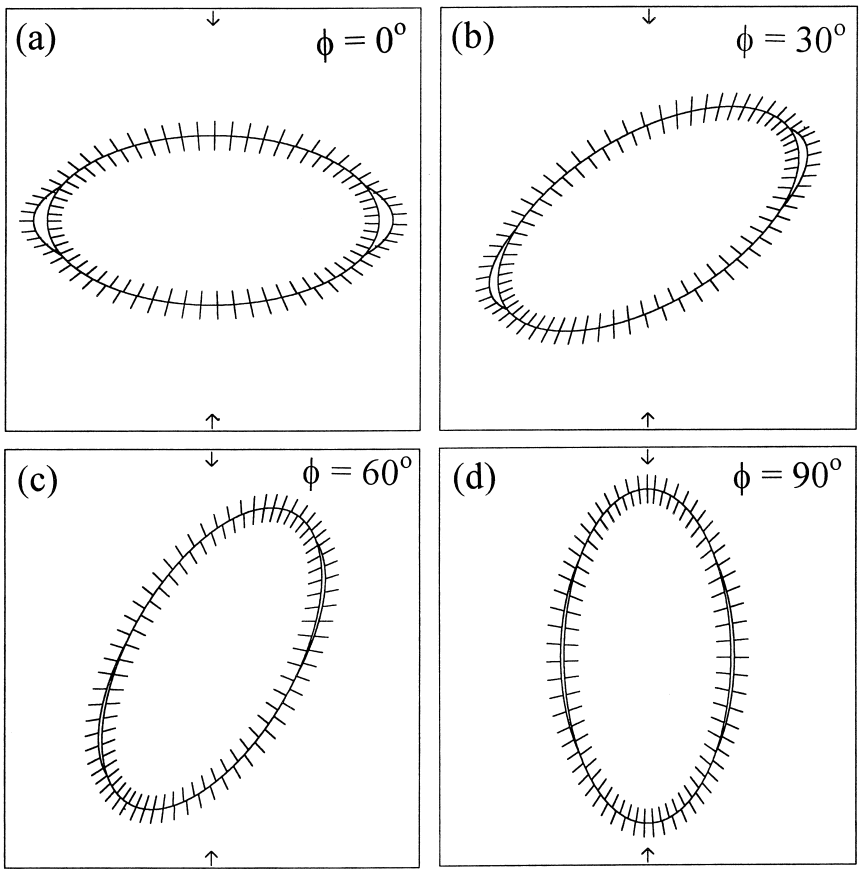

Fig. 4. Matrix detachment around elliptical inclusions in numerical models under pure shear. (a) $\phi = 0$; (b) $\phi = 30°$; (c) $\phi = 60°$ and (d) $\phi = 90°$. ϕ: initial inclination of the long axis of the inclusion to the bulk extension direction. Aspect ratio of inclusion (R) = 2.

fissures are asymmetrical, and located away from the long axis of the inclusion as well as the line parallel to the bulk extension direction and passing through the inclusion centre (Fig. 4b). The positional deviation of the fissures from the long axis of the inclusion is more pronounced as the inclination of the inclusion becomes large (Fig. 4c). In addition, the maximum separation between the matrix and inclusion decreases, and becomes a minimum when the inclusion is oriented with its long axis at a right angle to the bulk extension direction (Fig. 4d). However, in the latter case the fissures are symmetrical, with the line of maximum opening along the short axis. In the detachment zone there occurs two diametrically opposite points on either side of which the sense of slip (Modes 2 and 3) show reversal (Fig. 4). The matrix remains attached to the inclusion in particular locales, the positions of which also vary with the inclusion orientation ϕ (Fig. 4).

We computed numerically the surface area of locales of each mode of detachment as a function of inclusion orientation ϕ. The plot for $R = 2$ shows that the area of Mode 1 detachment varies monotonically with ϕ, and reaches a maximum value at $\phi = 90°$, and then decreases down to a minimum at $\phi = 180°$ (Fig. 5a). On the other hand, the variation in the area of slip (Mode 2) detachment shows ups and downs, showing maximum and minimum values at $\phi = 60$ and 120°, respectively. The area of intact inclusion–matrix interface is a maximum when the inclusion is oriented parallel to the bulk extension direction ($\phi = 0$), and progressively shrinks to a minimum when it becomes at a right angle to the extension direction ($\phi = 90°$). The plot overall indicates that, compared with Mode 1, slip detachment (Mode 2) occurs over a larger area of the inclusion–matrix interface.

Fig. 5b–d illustrates the effects of aspect ratio (R) on the variations of detachment areas versus inclusion orientation (ϕ). For $R \geq 5$, the area of Mode 1 detachment attains a peak value at $\phi = 45°$, and then decreases down to zero in a small range of ϕ near 60°, and finally varies steeply to reach a maximum peak value at $\phi = 90°$ (Fig. 5c). The interface area involving Mode 2 detachment shows peak values at $\phi = 45$ and 135°, which becomes progressively higher with increasing aspect ratio. These variations suggest that the detachment will take place solely in Mode 2 if the inclusion is oriented close to 60 or 120° with respect to the bulk extension direction. For $R \geq 10$, the area of Mode 1 detachment overall becomes much less compared with that of Mode 2 detachment, unless the inclusion is oriented at a high angle (75–105°) to the bulk extension direction (Fig. 5d). In addition, when the inclusion is oriented in the

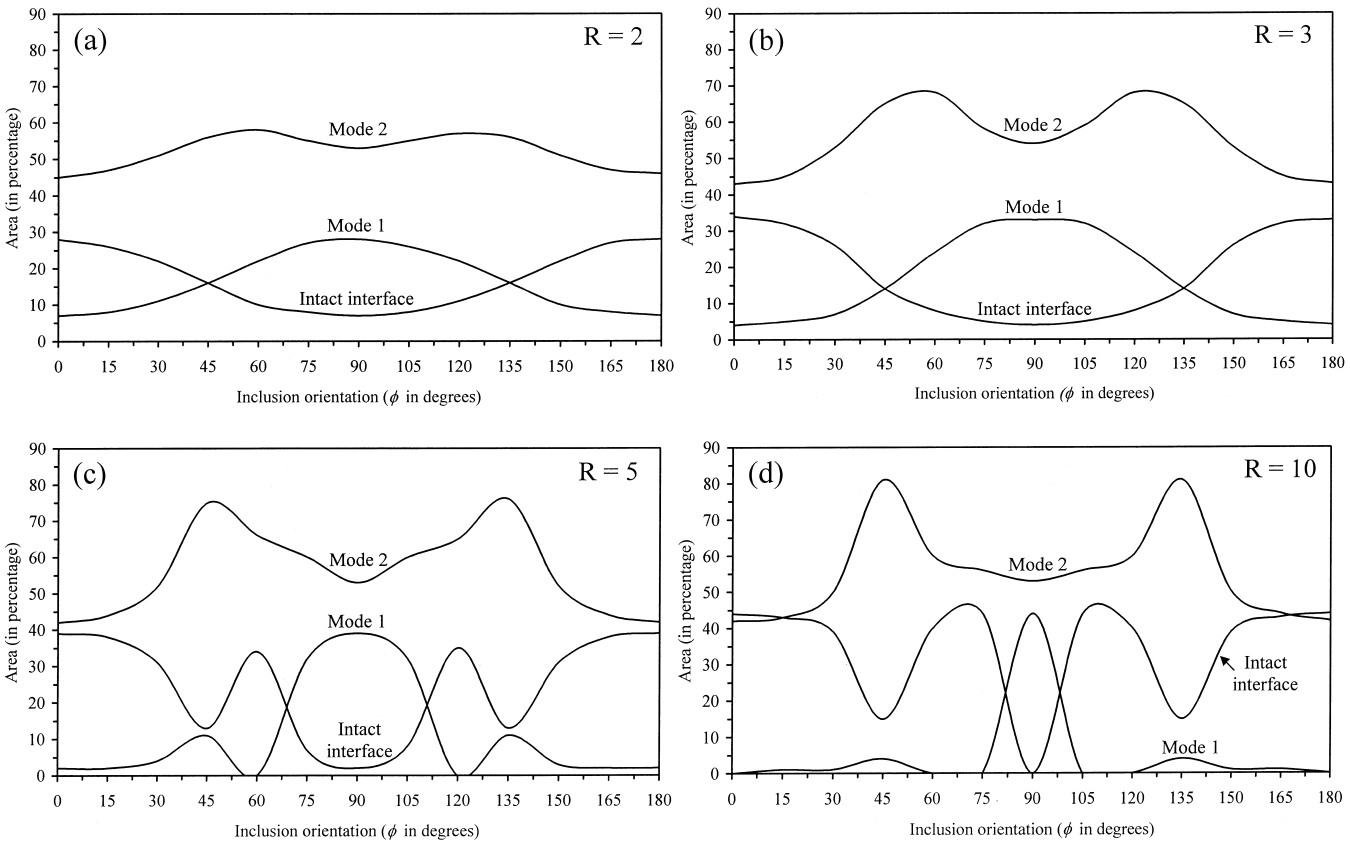

Fig. 5. Calculated plots showing variations in the area of fissure (Mode 1), slip (Mode 2) detachment and intact interface around an inclusion with its initial orientation ϕ. Bulk deformation is in pure shear. R: aspect ratio of inclusion. The area of Mode 3 is not shown here.

ranges of 60–75° and 105–120°, Mode 1 does not occur and the detachment takes place essentially in Mode 2.

We carried out another set of similar experiments under simple shear with circular (Fig. 6) and elliptical inclusions varying the initial inclination of the long axis of inclusion to the shear direction (ϕ) (Fig. 7). The experiments show that the detachment pattern for a given value of ϕ is similar to that obtained in pure shear with inclusion orientation $\phi - 45°$ to the bulk extension direction. However, this similarity is likely to be maintained for infinitesimal strains. Here we discuss only those aspects of numerical models that are pertinent to simple shear motion.

Circular inclusions ($R = 1$): Mode 1 detachment gives rise to symmetrical fissures on either side of the inclusion with the line of maximum opening oriented at an angle of 45° with the bulk shear direction (Fig. 6a). There are small parts on the inclusion boundary facing to the contraction field where the matrix remains attached to the inclusion. The sense of slip (Mode 2 detachment) on either side of it is synthetic and antithetic to the bulk shear sense (Fig. 6b).

Elliptical ($R = 2$) *inclusions*: when $\phi = 0$, Mode 2 detachment occurs over a major part of the inclusion boundary where the sense of slip is synthetic to that of the bulk shear (Fig. 7a). The matrix remains attached to the inclusion on two domains on either side of the inclusion located near the central shear plane. This intact part separates locales of Mode 2 detachment with synthetic and antithetic sense of slip. In the fissures Mode 3 operates on its either fringe with opposite sense of slip. Mode 2 detachment showing slip synthetic to bulk shear is dominant when the inclusion orientation ϕ is less than 45° or greater than 135° (Fig. 7a, b and f). On the other hand, for $45° < \phi < 135°$, Mode 2 with antithetic slip occurs dominantly at the interface (Fig. 7c–e).

The area of each mode of detachment at the inclusion–matrix interface is a function of inclusion orientation with respect to the shear direction, as in pure shear models. Fig. 8 shows the variations in the areas of the different modes with inclusion orientation (ϕ) for different aspect ratios (R).

3.3. Fields of detachment modes

For given mechanical strength of the inclusion–matrix interface, detachment cannot occur unless the inclusions attain a critical aspect ratio (R) or orientation (ϕ) with respect to the bulk flow direction. With the help of Eqs. (13) and (15) critical R or ϕ values were calculated and plotted as a function of the normalised values of tensile and shear strengths of the interface to find out the field of detachment in a $R - T_o^*, S_o^*$ space.

The plots (Fig. 9) show that circular inclusions ($R = 1$) in pure shear experience detachment with the matrix when the

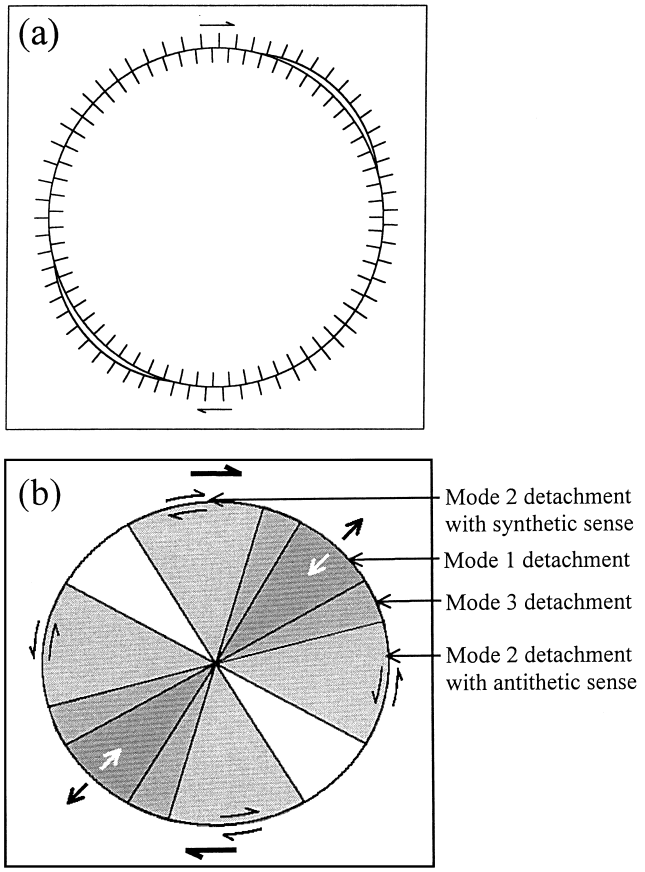

Fig. 6. (a) Pattern of detachment around circular inclusion in numerical model under simple shear. (b) Locales of Mode 2 detachment with opposite senses of slip on either side of the fissure detachment.

normalised values of S_o^* and T_o^* are less than two. That means, the strengths of the inclusion–matrix interface should not be greater than twice the bulk flow stress. On the other hand, when the inclusion is elliptical, the critical aspect ratios for Mode 1 and Mode 2 detachment to occur are functions of T_o^* and S_o^*, respectively, describing their fields in R versus S_o^*, T_o^* space (Fig. 9). The relations between R and S_o and T_o is different for different inclinations of the inclusion (ϕ) with the bulk extension direction (Fig. 9a–d). When $\phi = 0$ (Fig. 9a), both of them show more or less linear variations, indicating that the higher the mechanical strength of the inclusion–matrix interface the higher the critical aspect ratios are required for detachment to occur. The plots define a field delimiting the conditions in which detachment can occur solely in Mode 1, giving rise to fissures without any slip (Mode 2 detachment) between the inclusion and matrix. The plots also reveal the conditions favouring both Mode 1 and Mode 2 detachment, as observed in numerical models. It is found that for inclusion aspect ratio less than 10 the two modes of detachment can take place around an inclusion if S_o^* and T_o^* values are less than about five. When $\phi = 45°$ (Fig. 9b) the curves delimiting the fields of Mode 1 and Mode 2 detachment coincide with each other. They are non-linear, showing in overall negative gradients. The plots thus imply that detachment will essentially involve both Mode 1 and Mode 2, if the tensile and shear strengths of the inclusion–matrix interface are equal. Secondly, the critical aspect ratio required for detachment is inversely related to the mechanical strength of the interface. The two curves split from each other, as the inclusion orientation is larger than 45° (Fig. 9c). However, in contrast to the earlier case (i.e. $\phi < 45°$), the curve representing the critical conditions required for Mode 2 detachment lies above that of Mode 1, and the two curves thus define a field exclusively for Mode 2. The plots also reveal that, if the inclusion orientation is larger than 45° Mode 1 detachment can occur in inclusions irrespective of their aspect ratio when $T_o^* < 2$ (Fig. 9d).

We made a similar analysis of the fields for Mode 1 and Mode 2 detachment under simple shear deformation. The field patterns depend on the inclusion orientation to the simple shear direction. It was noticed that the results in simple shear for a certain inclusion orientation, say ϕ to the shear direction are identical to those in pure shear with inclination $\phi - 45°$ to the bulk extension direction.

4. Physical experiments

Simple physical model experiments were conducted under pure and simple shear to test the modes of inclusion–matrix detachment that are revealed from numerical simulations. The model consisted of a circular or elliptic cylindrical inclusion (rigid wax) hosted in a ductile matrix (putty with viscosity in the order of 10^4 Pa s). The cross-sectional face of the inclusion was exposed to the top surface of the putty block. The axis of the cylindrical inclusion was oriented along the axis of no-strain in the model. A set of parallel, passive marker lines was drawn across the inclusion and matrix interface to reveal the nature of detachment at the interface. Numerical simulations described in the previous sections indicate that the shape and orientation of inclusion and the mechanical strength of the inclusion–matrix interface are the principal parameters controlling the detachment pattern at the inclusion–matrix interface. In physical experiments we investigated only the effects of the first two geometrical factors.

Pure shear experiments with circular inclusions developed fissure (Mode 1) detachment on either side of the inclusion located along the central line parallel to the bulk extension direction and purely slip (Mode 2) detachment on either side of the fissures, as revealed from the offsetting of the markers (Fig. 10). This pattern of different modes of detachment around an inclusion matches that obtained from the numerical simulation (Fig. 10a). Elongate inclusions show varying detachment patterns with their initial inclusion orientation (Fig. 10b and c), and the nature of variation is consistent with that observed in numerical models (Fig. 4). Inclusions oriented parallel to the bulk extension direction developed symmetrical fissures (Mode 1)

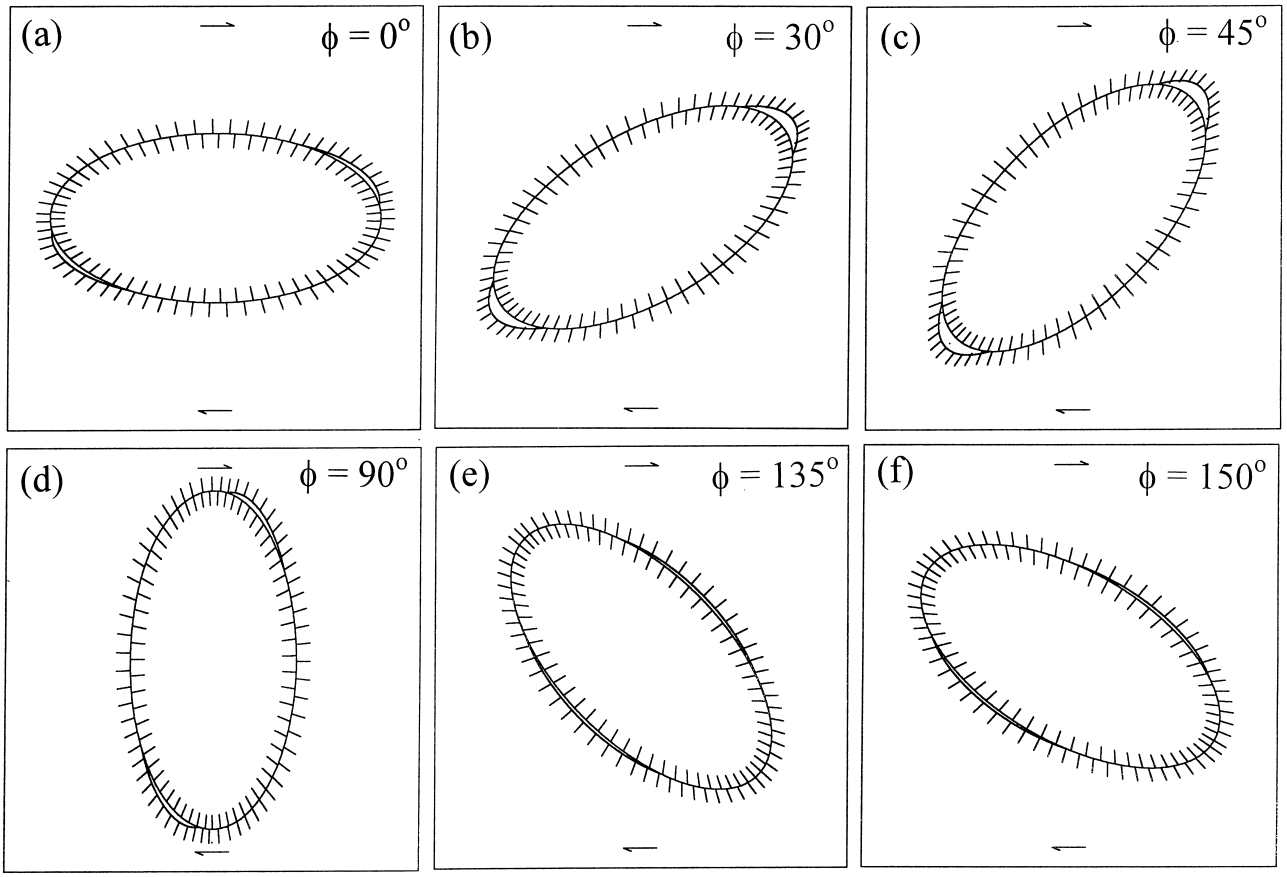

Fig. 7. Detachment around elliptical inclusions in numerical models under simple shear. ϕ is the initial inclination of the long axis of the inclusion to the bulk shear direction. $R = 2$.

of relatively small area, but large opening on either side of the inclusion (Fig. 10b). The fissures were located along the line parallel to the extension direction and passing to the inclusion centre. Slip detachment occurs over relatively a large area of the inclusion–matrix interface, compared with that around circular inclusions. Inclusions oriented oblique to the extension direction developed fissures with the lines of maximum opening located away from the long axis of the inclusion as well as the central line parallel to the bulk extension direction (Fig. 10c), as in the numerical model. With increase in inclination of the inclusion the magnitude of opening in the fissures progressively decreases and at the same time its area becomes large (Fig. 10d). We also carried out experiments on inclusions of varying aspect ratios, keeping all other conditions unchanged. The control of aspect ratio was most reflected in the development of fissures (Mode 1) around obliquely oriented inclusions. When inclusions were oriented at an angle of 45° with the extension direction, fissures had a tendency to die out with increase in aspect ratio (compare Fig. 10c and e). The theoretical result shows an inverse relation between the tensile strength of the inclusion–matrix interface and the aspect ratio of inclusion (Fig. 9b) when the inclusion is obliquely oriented with respect to the bulk extension direction. Thus, for a given mechanical strength Mode 1 detachment cannot take place if the aspect ratio is larger than a critical value, as observed in the physical model experiments. Similar experiments were conducted under simple shear deformation (Fig. 11), the result of which also agrees with the theoretical results, as can be revealed by comparing them with numerical models (Figs. 6 and 7).

5. Discussion

In the study of the inclusion–matrix system, the fundamental boundary condition that we need to deal with is: whether the inclusion–matrix interface is coherent or incoherent, as it has a significant control on the kinematic behaviour of the inclusions (Mancktelow et al., 2002) as well as the flow field around them (Pennacchioni et al., 2000). Many workers have modelled the flow fields and associated structures, such as porphyroclast tails, foliation drag around rigid inclusions, imposing parameters as a measure of degree of coherence between inclusion and matrix (Bjornerud and Zhang, 1995). The present study focuses mainly on the conditions under which the inclusion–matrix interface becomes incoherent, and experiences detachment. The results obtained from numerical simulations clearly indicate that the detachment does not

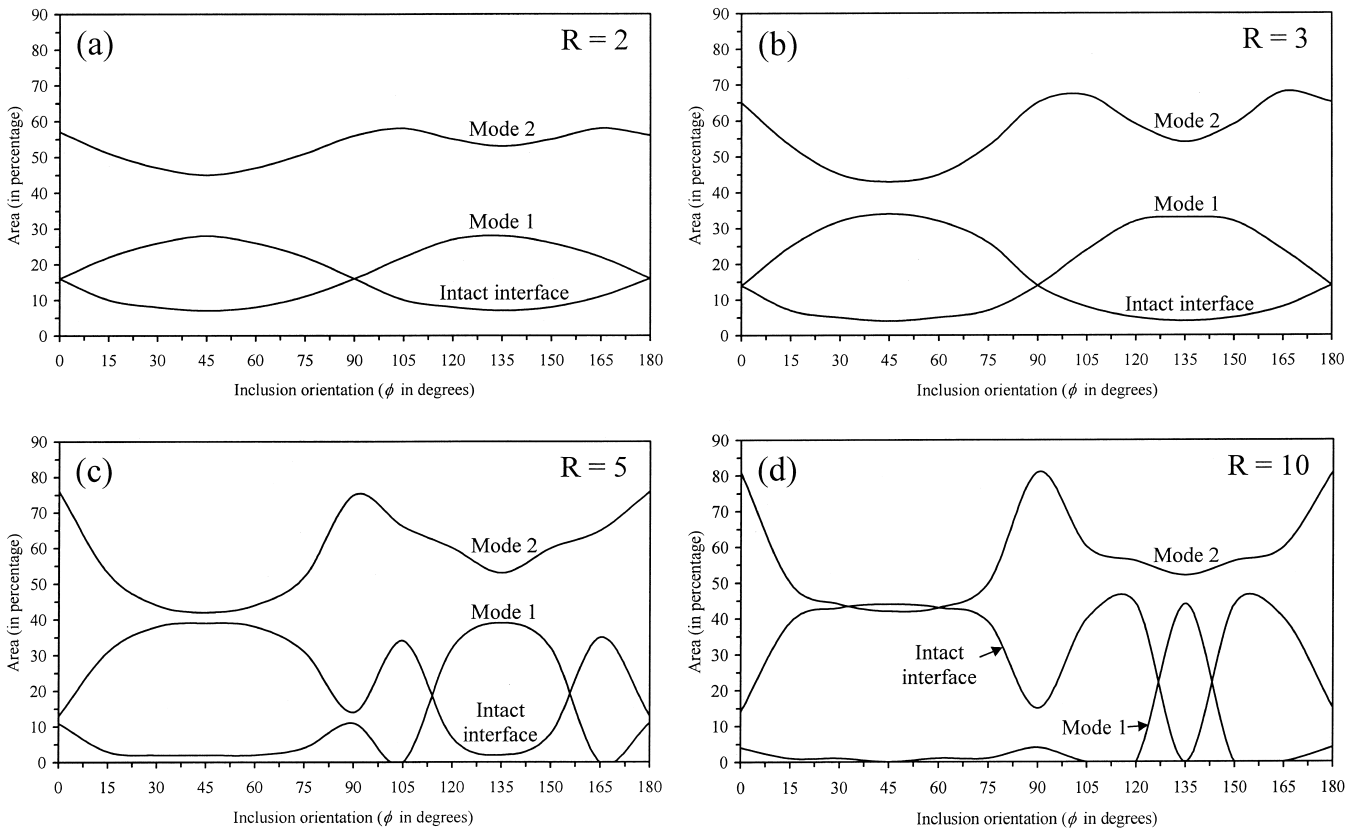

Fig. 8. Calculated plots showing variations in the area of fissure (Mode 1), slip (Mode 2) detachment and intact interface around an inclusion with its initial orientation ϕ. Bulk deformation is in simple shear. R: aspect ratio. The area of Mode 3 is not shown here.

occur uniformly around an inclusion, but are localized in particular domains involving three different modes. It therefore seems inappropriate in defining the degree of coherence using a single mathematical parameter, as attempted in earlier work (e.g. Bjornerud and Zhang, 1995). This analysis provides a first-hand basis in defining the detachment at the inclusion–matrix interface, which is necessary to interpret the behaviour of inclusions and, consequently, to use them as kinematic indicators in deformed rocks.

The shape and orientation of inclusion are found to be the most crucial parameters in determining the coherence to incoherence transformation at the inclusion–matrix interface. For a given strength, the interface becomes incoherent when the inclusion has a critical aspect ratio (Fig. 9a). Natural observation in mylonites shows that a deviation from the theoretical behaviour (Jeffery, 1922) only occurs for elongate inclusions with a critical aspect ratio. Inclusions exceeding this aspect ratio stabilize to particular positions. Our analysis confirms that detachment develops preferentially at the interface of inclusions with large aspect ratios under a specific orientation, affecting their kinematic behaviour (Pennacchioni et al., 2001; Mancktelow et al., 2002; ten Grotenhuis et al., 2002).

The analysis in this paper is based on several considerations, which need to be addressed:

1. The detachment patterns have been demonstrated in numerical models, considering the tensile strength T_o and shear strength S_o of the inclusion–matrix interface independently. The same analysis could be made imposing a failure criterion. In this analysis, however, we intentionally avoid using any particular failure criteria, e.g. Coulomb–Navier criterion or Griffith's criterion, as they define the conditions of failure in a single, continuous body. We are, however, sceptical whether they are applicable to characterise the detachment at the interface between two distinctly different materials, i.e. rigid inclusion and ductile matrix. We actually deal with the bonding strength between the materials, the stress required to break the adherence between the two materials. Now, one can break the bond by applying critical shear or tensile stresses, what we consider here as S_o and T_o. The interface will be on the verge of developing fissures (Mode 1 detachment) where the normal stresses exceed T_o. On the other hand, this will have a tendency to show slip where the shear stresses exceed S_o. However, the slip movement subsequently depends on other factors, e.g. the frictional property of the interface. This aspect has not been taken into consideration because it is difficult to apply a friction law, which is strictly valid on fractures in the brittle regime. The pattern of Mode 2 detachment may be

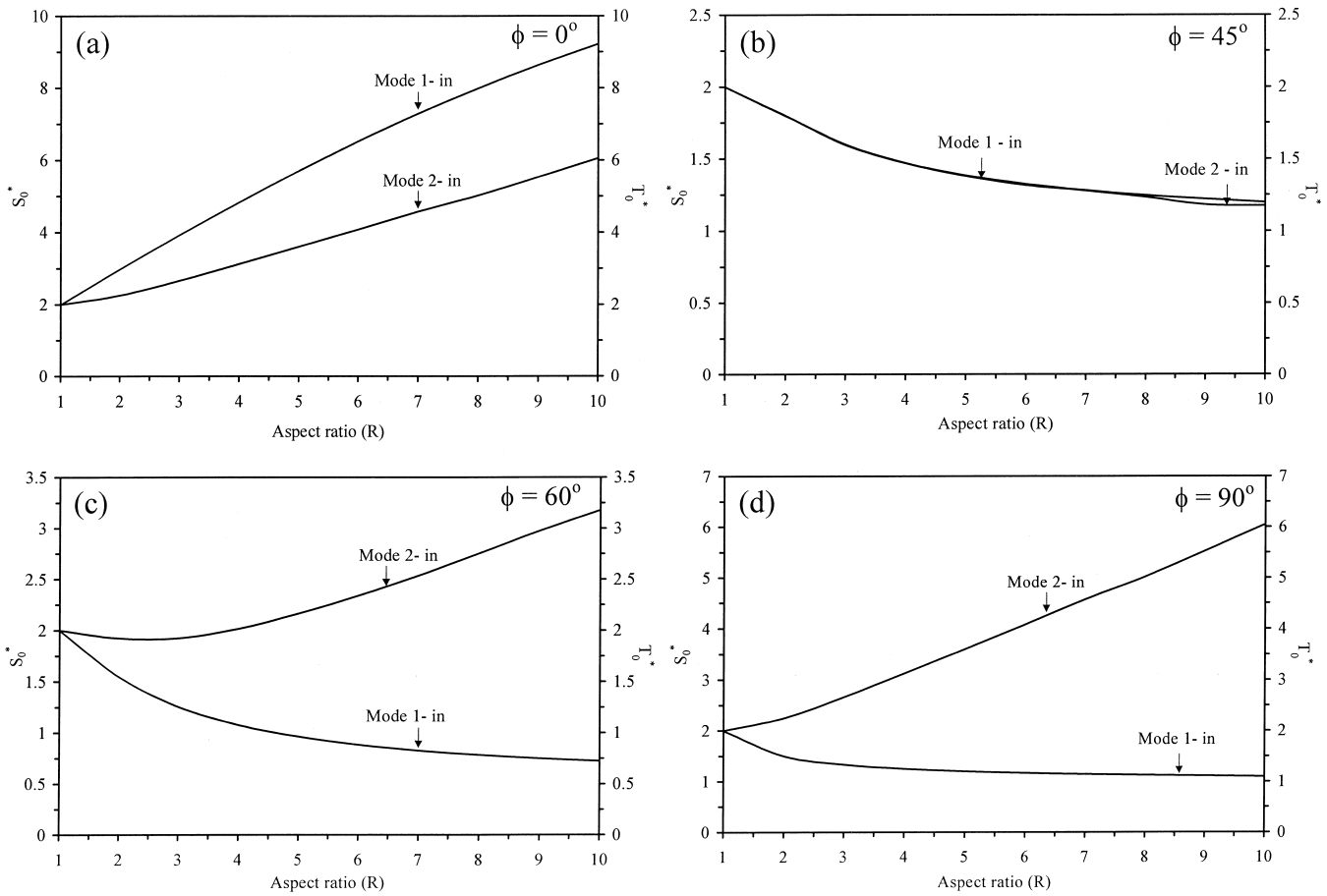

Fig. 9. Variations of critical aspect ratios, delimiting the fields of no-detachment and Mode 1 and Mode 2 detachment, as a function of normalised values of tensile strength (T_o^*) and shear strength (S_o^*) of the inclusion–matrix interface, respectively. The deformation is under pure shear. ϕ is the inclination of the long axis of inclusion to the bulk extension direction.

different from those presented here, as it will depend upon the normal stress component in case of frictional condition.

2. The mechanical strengths of the interface have been chosen arbitrarily as $S_o = T_o = 1$. This is merely to demonstrate the disposition of three modes of detachment around an inclusion more elegantly. In natural conditions S_o and T_o may be different, giving rise to different patterns of detachment. For example, when $S_o \gg T_o$, inclusions will not develop Mode 2 detachment, as evident from the field diagrams (Fig. 9). On the contrary, the inclusion–matrix will be affected entirely by Mode 1, giving rise to only fissure detachment. Thus, there may be different combinations of detachment around an inclusion depending upon different values of S_o and T_o, which can be predicted from the field diagrams of detachment (Fig. 9). However, the main aim in presenting these numerical simulations is to illustrate how an inclusion may experience detachment in different modes and what may be the probable geometrical disposition of the different modes on the inclusion–matrix interface, and how they depend on the shape and orientation of the inclusion.
3. In our analysis we deal with cases where the normal stress acting at the inclusion–matrix interface is larger than the confining pressure, and the effective normal stress reaches the tensile strength of the interface, giving rise to Mode 1 (fissure) detachment. It is evident from

Fig. 10. Matrix detachment around rigid inclusions in physical models under pure shear. Markers were drawn parallel to the direction of bulk shortening across the inclusion–matrix boundary to reveal the detachment pattern. They developed drag patterns under the heterogeneous matrix flow around the inclusions (cf. Mandal et al., 2001a). (a) Circular inclusion showing development of symmetrical fissures (Mode 1) along the central line parallel to the bulk extension direction and slip detachment (Mode 2) on either side of the fissures. (b)–(d) Elliptical inclusions with aspect ratio $R = 2$ and initial orientation $\phi = 0$, 45 and 90°, respectively. Note that in (c) the inclusion has rotated and lowered the inclination of its long axis with the bulk extension direction, and also that the fissure (Mode 1 detachment) is located away from both the long axis of the inclusion and the central line parallel to extension direction. (e) Elongate inclusions with aspect ratio $R = 3$ and initial orientation $\phi = 45°$. Note that slip (Mode 2) is the dominant detachment mode at the inclusion–matrix interface and Mode 1 detachment is virtually absent.

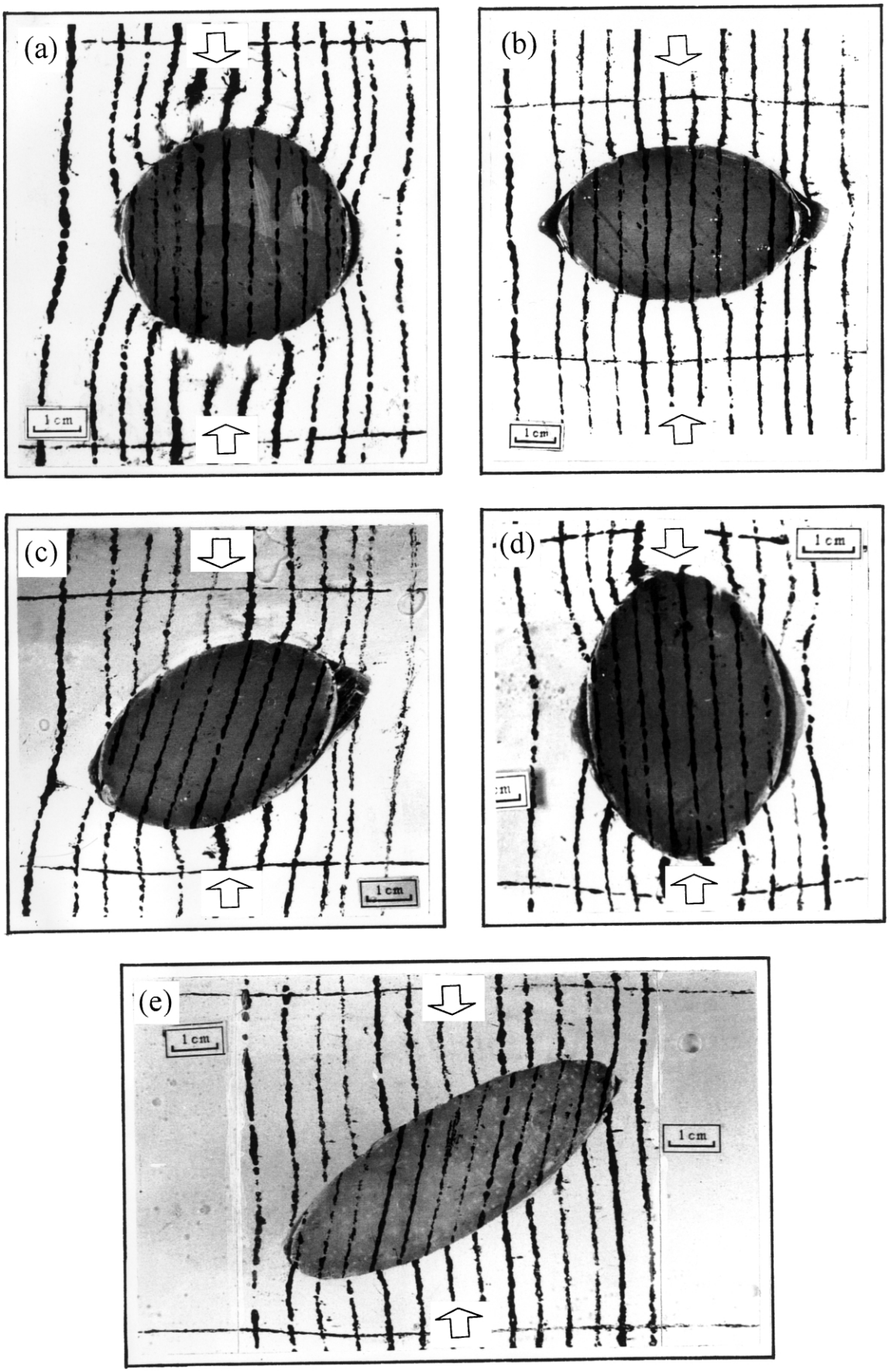
(a)
1 cm
(b)
1 cm
(c)
1 cm
(d)
1 cm
(e)
1 cm
1 cm

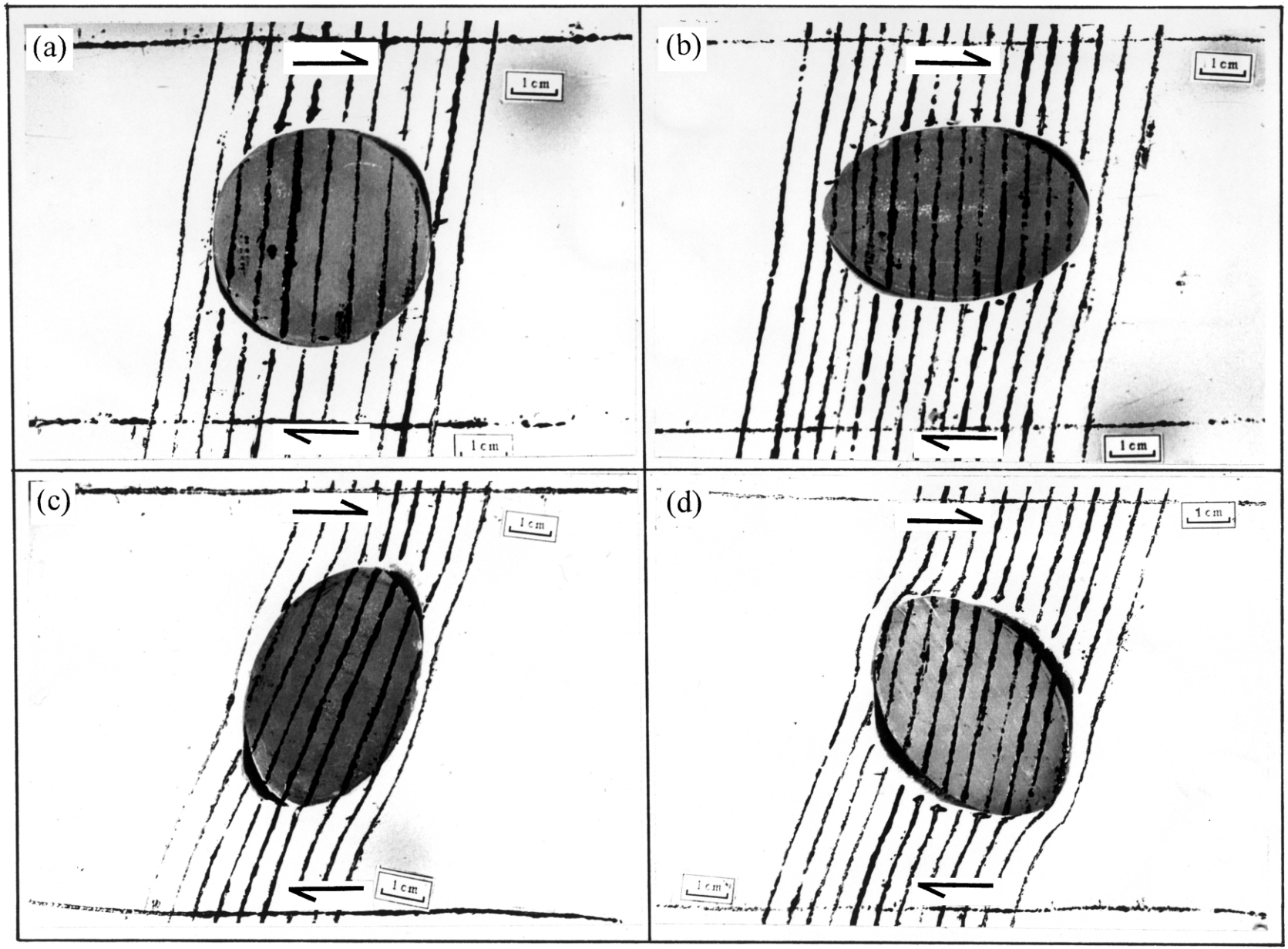

Fig. 11. Matrix detachment around rigid inclusions under simple (dextral) shear bulk deformation. (a) Circular inclusions showing Mode 1 fissures with maximum opening in the direction of 45° with the shear direction and Mode 2 (slip) detachment. (b)–(d) Elliptical inclusions, initially oriented parallel (b), perpendicular (c) and at an angle of 135° (d) with the shear direction. Note that the location of fissures (Mode 1 detachment) varies with change in inclusion orientation, and that slip (Mode 2) detachment becomes dominant when the inclusion is oriented parallel to the bulk shear direction.

Eqs. (13) and (15) that the normal stress everywhere at the interface will be compressive if the confining pressure is very large, and is thus unlikely to form Mode 1 detachment. This analysis is primarily aimed at demonstrating the influence of inclusion geometry on the detachment processes under a condition of confining pressure allowing Mode 1 detachment. This is relevant to natural inclusion–matrix systems, which generally show a wide variation in the shape and orientation of inclusions. Our analysis is applicable to explain the variation in detachment pattern in such a system, where the confining pressure can be considered as a constant parameter.

There are some limitations in the present theoretical and experimental approach. Firstly, the entire analysis is based on two dimensions, considering that the axis of rotation remains in coincidence with the axis of no-strain, which may not always be so in the natural conditions. Secondly, there are a number of simplistic assumptions in the analysis. Numerical simulations consider ideally the displacement at a point on the interface as a linear function of the stress acting at that point. Similarly, the matrix is assumed to be Newtonian, and mechanically isotropic during the deformation. In natural conditions there may large departures from these assumptions. Thirdly, the theoretical model is valid for infinitesimal strain till the inclusion–matrix interface becomes incoherent. This is not applicable in tracking the detachment subsequently in the course of progressive deformation.

6. Conclusions

1. The detachment at an inclusion–matrix interface may occur in diverse modes: Mode 1—the matrix is separated from the inclusion with displacement normal to the inclusion boundary; Mode 2—the matrix slips on the surface of the inclusion; and Mode 3—the detachment occurs by a combination of the above two modes. Besides the mechanical strength of the interface, other physical factors controlling the modes of detachment and their geometrical patterns are the aspect ratio and orientation of the inclusion.
2. Circular inclusions ($R = 1$) can show detachment if the normalised values of the mechanical strength of the interface is less than two. Under such conditions both Mode 1 and Mode 2 detachment can occur, giving rise to fissures along the central line parallel to the bulk extension in the case of pure shear and along a line at an angle of 45° with the shear direction in the case of simple shear, and slip zones on either side of the fissures.
3. For given inclusion orientation (ϕ), the conditions for detachment around elliptical inclusions are different for different modes, and are functions of aspect ratio of the inclusions. In pure shear deformation, when $\phi = 0$ the critical aspect ratio at which detachment can take place is directly proportional to the mechanical strength of the inclusion–matrix interface. On the other hand, this is inversely proportional to the mechanical strength, when $\phi = 45°$. For $\phi > 45°$ the aspect ratio required for Mode 1 detachment is inversely proportional, whereas that for Mode 2 is directly proportional to the mechanical strength of the interface.
4. Irrespective of the orientation of inclusion, detachment is unlikely to occur if the mechanical strength of the interface normalised to the bulk flow stress is larger than six and the aspect ratio is less than 10.

Acknowledgements

We wish to thank two anonymous reviewers for their detailed comments on the early version of the manuscript. We are grateful to Prof. C.W. Passchier for giving suggestions in revising the manuscript. We also thank Nibir Mandal and Chandan Chakraborty for their discussions and suggestions on this work. The CSIR, India is gratefully acknowledged for providing financial supports.

References

Bjornerud, M.G., 1989. Mathematical model for folding of layering near rigid inclusions in shear deformation. Journal of Structural Geology 11, 245–254.

Bjornerud, M.G., Zhang, H., 1995. Flow mixing inclusion matrix coherent mantle growth and the development of porphyroclast tails. Journal of Structural Geology 17, 1347–1350.

Gay, N.C., 1968. Pure shear and simple shear deformation of inhomogeneous viscous fluids. 1. Theory. Tectonophysics 5, 211–234.

Ildefonse, B., Mancktelow, N.S., 1993. Deformation around rigid particle: influence of slip at the particle/matrix interface. Tectonophysics 221, 345–359.

Jeffery, G.B., 1922. The motion of ellipsoidal particles immersed in a viscous fluid. Proceedings of the Royal Society of London A 102, 161–179.

Kenkmann, T., Dresen, G., 1998. Stress gradients around porphyroclasts: palaeo-piezometric estimates and numerical modelling. Journal of Structural Geology 20, 163–173.

Mancktelow, N.S., Arbaret, L., Pennacchioni, G., 2002. Experimental observations on the effect of interface slip on rotation and stabilisation of rigid particles in simple shear and a comparison with natural mylonites. Journal of Structural Geology 24, 567–585.

Mandal, N., Samanta, S.K., Chakraborty, C., 2001a. Numerical modeling of heterogeneous flow fields around rigid objects with special reference to particle paths, strain shadows and foliation drag. Tectonophysics 330, 177–194.

Mandal, N., Chakraborty, C., Samanta, S.K., 2001b. Controls on the failure mode of brittle inclusions hosted in a ductile matrix. Journal of Structural Geology 23, 51–66.

Masuda, T., Ando, S., 1988. Viscous flow around a rigid spherical body: a hydrodynamical approach. Tectonophysics 148, 337–346.

Masuda, T., Mizuno, N., 1996. Computer modeling mantled porphyroclasts in Newtonian and non-Newtonian simple shear viscous flows. Journal of Structural Geology 18, 1487–1491.

Passchier, C.W., 1994. Mixing in flow perturbations: a model for

development of mantle porphyroclasts in mylonites. Journal of Structural Geology 16, 733–736.

Pennacchioni, G., Fasolo, L., Cecchi, M.M., Salasnich, L., 2000. Finite-element modeling of simple shear flow in Newtonian and non-Newtonian fluids around circular rigid particle. Journal of Structural Geology 22, 683–692.

Pennacchioni, G., Toro, G.D., Mancktelow, N.S., 2001. Strain-insensitive preferred orientation of porphyroclasts in Mont Mary mylonites. Journal of Structural Geology 23, 1281–1298.

Ramsay, J.G., Huber, M.I., 1983. The Techniques of Modern Structural Geology. Volume 1: Strain Analysis, Academic Press, London.

Ramsay, J.G., Lisle, R.J., 2000. The Techniques of Modern Structural Geology. Volume 3: Continuum Mechanics in Structural Geology, Academic Press, London.

ten Grotenhuis, S.M., Passchier, C.W., Bons, P.D., 2002. The influence of strain localisation on the rotation behaviour of rigid objects in experimental shear zones. Journal of Structural Geology 24, 485–499.